Journal of Electroceramics, 12, 7–17, 2004
© 2004 Kluwer Academic Publishers. Manufactured in The Netherlands.

Thin Film Piezoelectrics for MEMS

S. TROLIER-MCKINSTRY [1] & P. MURALT [2]

[1] *Materials Research Institute and Materials Science and Engineering Department, Penn State University*

[2] *Ceramics Laboratory, Swiss Federal Institute of Technology EPFL, Lausanne, Switzerland*

Abstract. Thin film piezoelectric materials offer a number of advantages in microelectromechanical systems (MEMS), due to the large motions that can be generated, often with low hysteresis, the high available energy densities, as well as high sensitivity sensors with wide dynamic ranges, and low power requirements. This paper reviews the literature in this field, with an emphasis on the factors that impact the magnitude of the available piezoelectric response. For non-ferroelectric piezoelectrics such as ZnO and AlN, the importance of film orientation is discussed. The high available electrical resistivity in AlN, its compatibility with CMOS processing, and its high frequency constant make it especially attractive in resonator applications. The higher piezoelectric response available in ferroelectric films enables lower voltage operation of actuators, as well as high sensitivity sensors. Among ferroelectric films, the majority of the MEMS sensors and actuators developed have utilized lead zirconate titanate (PZT) films as the transducer. Randomly oriented PZT films show piezoelectric $e_{31,f}$ coefficients of about -7 C/m^2 at the morphotropic phase boundary. In PZT films, orientation, composition, grain size, defect chemistry, and mechanical boundary conditions all impact the observed piezoelectric coefficients. The highest achievable piezoelectric responses can be observed in $\{001\}$ oriented rhombohedrally-distorted perovskites. For a variety of such films, $e_{31,f}$ coefficients of -12 to -27 C/m^2 have been reported.

Keywords: piezoelectrics, MEMS, thin films, orientation

Introduction

The field of MEMS is a large and growing one, with numerous means reported for both sensing and actuation on-chip. Given the plethora of mechanisms by which the environment can be detected and/or useful responses made, it is worth considering the impetus for integrating piezoelectric thin films into MEMS devices (i.e. what advantages offset the need to introduce new materials into the cleanroom environment?). As usual, the answer to such a question depends significantly on the device or function in question. However, a couple of attributes come to the fore in promoting the use of piezoelectric devices in MEMS applications. These include:

(1) The relatively straightforward manner in which high frequency resonant structures, with good temperature stability, can be implemented. At present there is a substantial research effort in developing MEMS devices with high electrical quality factors for rf circuits. Low frequencies are straightforward to obtain via MEMS techniques [1, 2]. While considerable progress has been made recently in the development of electrostatically actuated devices with high resonant frequencies [3, 4], these devices are inherently rather small, require sophisticated patterning techniques, and are susceptible to mass-loading changes on environmental exposure. In contrast, piezoelectric resonators with resonant frequencies in the high MHz–GHz range are widely used in scanning acoustic microscopes [5], and have seen considerable development in thin film bulk acoustic resonators (FBAR) [6, 7].

(2) Piezoelectric sensors do not require power themselves (although of course any associated electronics such as charge or voltage amplifiers, etc., will need to be powered). As a result, piezoelectric MEMS are interesting for low power requirement sensors. Indeed, in situations where the sensor is operated only on an intermittent basis, it is also possible to visualize using any such sensor in a mechanically noisy environment as a power source

the remainder of the time. Such energy harvesting schemes have been implemented in bulk and thick film piezoelectrics [8–11]. Moreover, as sensors, it is possible to design piezoelectric devices with broad dynamic range and low noise floors.

(3) The ability to perform large amplitude actuation with lower drive voltages and low hysteresis. The preponderance of MEMS literature utilizes electrostatic actuation of flexural structures. Electrostatics is relatively easy to implement, and offers the possibility of large amplitude actuation, though typically at the cost of large driving voltages and substantial hysteresis. Current-based actuation approaches, such as those utilized in many thermal and magnetically driven devices, typically require high power to operate, and in some cases are inherently slow (e.g. due to thermal time constants). In contrast, the piezoelectric effect can be utilized to drive large displacements in MEMS structures at modest voltages, low powers, and with low hysteresis.

(4) The fact that piezoelectricity shows good scaling with size. That is, the energy density available for actuation remains high, even as device sizes drop. Poor scaling is, of course, one of the principal reasons that electromagnetic motors are not attractive at MEMS size scales.

(5) The straightforward ability to provide electrical signals to drive or sense the device. Much like the case of electrostatics, piezoelectrics need only electrical contact for sensing or actuation. From the point of view of electronic circuit design, piezoelectric elements are CMOS compatible. The resulting signals are easily processed on chip.

With these advantages, there are some application areas where integration of piezoelectric films into the device becomes practical. Considerable progress has been made in this area over the last 20 years, with devices such as filters, micromotors, micropumps, micro-sonar arrays, scanning force microscopy tips, accelerometers, etc. [12–17] having been demonstrated.

Important Piezoelectric Coefficients for MEMS

Parameters needed for the description of the piezoelectric effect in a body with homogeneous properties on the scale of its dimensions are the strain tensor x_i (where $i = 1$ to 6 in reduced notation [18]), the stress tensor σ_i ($i = 1$ to 6), as well as the electric field E_i and the electric displacement field D_i ($i = 1$ to 3) vectors. Piezoelectricity means that there is a linear relation between the D-field and strain/stress:

$$D_i = \sum_k d_{ik}\sigma_k \quad \text{or} \quad D_i = \sum_k e_{ik}x_k \tag{1}$$

These equations describe the so-called direct effect. The piezoelectric coefficients d_{ik} and e_{ik} are the components of a 3rd rank tensor, which in reduced tensor notation corresponds to a 3×6 matrix. The d and e coefficients are related to each other through the stiffness tensor $c_{ij}^E : d_{ik} = e_{ip}c_{pk}^E$. The converse effect is described by the same set of piezoelectric coefficients:

$$x_i = \sum_k d_{ki}E_k \quad \text{or} \quad \sigma_i = -\sum_k e_{ki}E_k \tag{2}$$

Piezoelectricity (see [19]) occurs in crystal classes containing no center of inversion (it is also forbidden in crystal class 432). In some piezoelectric crystal classes there exists a polar axis. All the piezoelectrics used in thin film form belong to this material group. (Quartz, which has no polar axis, is only a useful piezoelectric in single crystalline form). It is conventional to assign the coordinate index 3 to the polar axis direction, and to define d_{33} as a positive quantity.

In MEMS technology, most of the piezoelectric thin films are and will be polycrystalline materials. The piezoelectric effect is averaged over all the grains. At this point one has to distinguish between ferroelectric and non-ferroelectric polar materials. The latter do not allow reorientation of the polar axis. In this case, the material growth process has to provide for a textured structure that includes the alignment of the polar directions. In ferroelectric materials, the polar axis can be reoriented by an electric field. In these materials, an internal electrical polarization, i.e. the spontaneous polarization, is observed. By means of poling, i.e. the application of a large electric field able to switch the polarization, the polarization component parallel to the poling field is aligned. As a result, there is a net piezoelectric effect. In ceramics, it is conventional to assign the index 3 to this poling direction. For the case of vertically stacked capacitor structures (see Fig. 1(a)), direction 3 is perpendicular to the film plane, using the same convention as for polycrystalline ferroelectrics. The piezoelectric coefficient d_{33} thus describes the piezoelectric

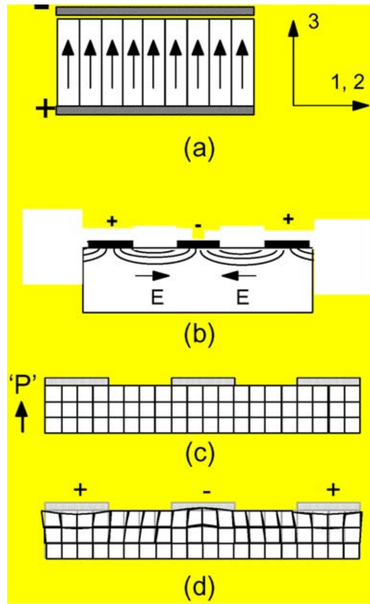

Fig. 1. Electrode systems for driving piezoelectric films: (a) Planar capacitor structure with top and bottom electrodes. (b) Electric field with interdigital electrodes. (c) Case of polar film with uniform perpendicular polarization. (d) Schematic drawing of strains induced by d_{15} between the electrodes, and d_{33}, d_{31} below the electrodes.

effect in the out-of-plane direction, as e.g., the thickness change of the free film. The directions 1 and 2 are therefore in the plane of the film. In a polycrystalline film, these directions are equivalent. This means that the in-plane strains due to E_3 are isotropic and d_{31} and d_{32} are the same. The shear strain coefficients d_{15} and d_{14} are equal as well: $x_5 = d_{15}E_1$, $x_4 = d_{14}E_2$. The polycrystalline thin film geometry thus recovers the cylindrical symmetry of poled ceramics, yielding the same three independent elements of the piezoelectric tensor as for tetragonal symmetry ([18]), i.e. d_{33}, d_{31}, d_{15}. In the case of non-ferroelectric materials, the polar crystal axis is by convention the "3" axis as well. In order to profit from a maximal longitudinal and transverse response (d_{33} and d_{31}), the film orientation must be (001) or (00-1). The two possibilities have opposite piezoelectric responses! Uniform texture of either of the two possibilities has thus to be achieved. In Fig. 1(a), the arrows symbolize the direction of the polar axis in a non-ferroelectric system such as AlN and ZnO, or the average polarization per grain in a poled ferroelectric material. The in-plane directions are again equivalent if the film is polycrystalline, or if the polar axis is a threefold or higher rotation axis. In both cases, the resulting symmetry is thus again the same as for poled ceramics. Polar films also offer the possibility to work with shear strains (if the film is ferroelectric it needs to be poled; using the same electrodes for poling and operation, the field is always parallel to the polarization). In between interdigital electrodes [20] the field lies in the film plane (electric field in 1 and 2 directions: E_1, E_2), thus perpendicular to the polar axis. The resulting shear strains add to the strains of d_{33} and d_{31} below the electrodes, as shown in Fig. 1. The result is an alternating compression and dilatation of the surface layer. At a given frequency, surface acoustic waves are excited whose wavelength is defined by the period of the interdigital electrode. The nature of the wave depends on a large number of parameters of the piezoelectric film, other involved layers and the substrate. The main interest in the use of piezoelectric films is to excite SAW waves in non-piezoelectric materials with high SAW velocities such as sapphire [21] and diamond [22, 23] in order to realize high frequency RF filters. To some extent it is also possible to sputter polar films with an oblique incidence of the atom flux onto the substrate. The polar axes consequently grow inclined to the substrate normal [24] and shear strains are excited even in the planar capacitor geometry. Shear coefficients are more difficult to access in ferroelectric films, as the polarization direction follows always the poling field, which has the same geometry as the operating field when the corresponding electrodes are the same.

The main difference between thin film and bulk materials lies in the fact that thin films are used in a composite structure, where the total elastic properties are often dominated by the other part of the structure. This other part may be a silicon cantilever, a silicon oxide or a nitride membrane, for instance. The interaction with the substrate is very anisotropic. At the interface along the in-plane directions (indices 1, 2), the piezoelectric thin film and the substrate have identical strains. Perpendicular to the film plane, the thin film is free to move, i.e., $\sigma_3 = 0$. As a consequence, there is no deformation mode in which only one piezoelectric coefficient is involved. The complete equation of state needs to be analyzed. For illustration, a thin film clamped to a much thicker substrate is considered (i.e. a piezoelectric laminated plate). When a field is applied, the strains in the plane stay at zero ($x_1 = x_2 = 0$); in-plane stresses and an out-of-plane strain are developed. The equation of state using the compliance tensor and d coefficients reads now as (for the average polar direction

parallel to E-field: no shear components):

$$x_1 = (s_{11}^E + s_{12}^E)\sigma_1 + d_{31}E_3 = 0$$
$$x_3 = 2s_{13}^E\sigma_1 + d_{33}E_3 \quad (3)$$

The first line of Eq. (3) allows derivation of the in-plane stresses, that is an effective $e_{31,f} = -\sigma_1/E_3$. The second line leads to the definition of an effective $d_{33,f} = x_3/E_3$:

$$e_{31,f} = \frac{d_{31}}{s_{11}^E + s_{12}^E}$$
$$d_{33,f} = d_{33} - \frac{2s_{13}^E}{s_{11}^E + s_{12}^E} d_{31} \quad (4)$$

Equivalent expressions can be derived using the e-coefficients. Both effective coefficients can be measured directly. It turns out that $d_{33,f}$ is always smaller than d_{33} and that the absolute value of $e_{31,f}$ is always larger than that of e_{31}.

The input and output parameters for actuator and sensor applications of piezoelectric laminated plates is schematically described in Fig. 2. In an actuator, application of a voltage leads to a piezoelectric in-plane stress causing a deflection of the structure, whereas the piezoelectric thin film is strained in the out-of-plane direction. In the sensor mode, in-plane strains create the piezoelectric charges that record the deformation of the flexible structure. In addition, the film is sensitive to out-of-plane stress (which also causes in-plane strain!).

A cantilever structure can be modelled by analytical methods [25, 26]. In the actuator mode, a constant curvature is established at a given voltage. The deflection at the end of the beam is proportional to the square of the beam length. Excursions of 10 to 20 μm with 500 μm long beams have been obtained [27]. More complicated structures must be analyzed by means of finite element calculations [28].

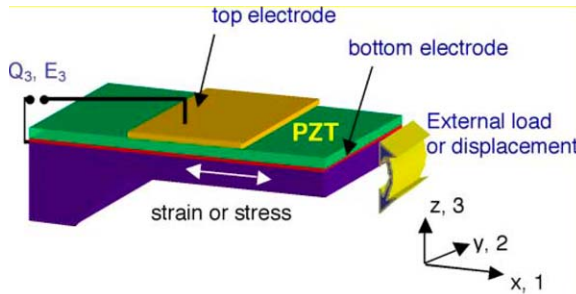

Fig. 2. Input (E_3, load) and output parameters (displacement, Q_3) in actuator and sensor applications for piezoelectric laminated plates.

Table 1. Figures of merit for piezoelectric sensors (limited by signal to noise ratio).

Physical parameter	Figure of merit
Deflection force, piezoelectric charge of deflected piezoelectric laminated structure	$e_{31,f}$
Piezoelectric voltage in deflected piezoelectric laminated structure	$e_{31,f}/\varepsilon_0\varepsilon_{33}$
Coupling coefficient for plate wave	$e_{31,f}^2/\varepsilon_0\varepsilon_{33}$
Coupling coefficient for thickness wave	$e_{33}^2/(\varepsilon_0\varepsilon_{33}c_{33}^D) \approx d_{33,f}^2 \cdot c_{33}^E/\varepsilon_0\varepsilon_{33}$
Signal-to-noise ratio	$e_{31,f}(\varepsilon_0\varepsilon_{33}\tan\delta)^{-1/2}$

The piezoelectric coefficients are not the only material parameters of interest. In addition to force, deflection and piezoelectric charge (current), other performance issues are important. In resonating structures the coupling coefficient (k^2) is essential. It describes the effectiveness of energy transformation from electrical to mechanical energy. Part of the electrical energy is dissipated and transformed to heat. The dielectric loss angle ($\tan\delta$) is involved in this phenomenon. The dielectric loss also generates a noise current or voltage, which imposes limits to the resolution, or more precisely, to the signal-to-noise-ratio of sensors. Whether the intrinsic noise due to $\tan\delta$ limits the performance or not depends on the application, electronics, and external noise levels. Table 1 summarizes the figures of merit for the various criteria. Note that the figure of merit for intrinsic signal-to-noise ratio does not depend on whether voltage or current is detected.

AlN and ZnO

Both AlN and ZnO are wurtzite structured materials which show a piezoelectric response along [0001]. For MEMS applications, ZnO and AlN are commonly sputter deposited [29, 30]. ZnO is preferentially deposited at room temperature in order to obtain a high resistivity. AlN does not exhibit conductivity problems and good films are reported to grow between 100 and 900°C. A convenient temperature for sputter tools as well as for

applications is the range of 200 to 400°C [31]. Essential for achieving good piezoelectric coefficients is the homogeneous nucleation of grains with (0001) texture of the same polar direction. It appears that a more perfect {0001} texture, as determined by X-ray diffraction (no peaks of other orientations, small rocking curve width) includes as well a better selectivity between the (0001) and $(000\bar{1})$ versions. In other words, the same growth mechanisms leading to a more perfect (0001) texture and crystalline quality lead also to a preferential growth of one of the polarizations. A first indication of such phenomena was found by Hickernell and coworkers [32] when they observed that the SAW transducer loss was smaller when the X-ray peak width was smaller. More recently, a clear correlation was established between the coupling coefficient of a BAW resonator and the rocking curve width of the AlN film [33]. Evaluating $d_{33,f}$ of AlN as a function of various deposition conditions, it was observed that the most important parameter influencing the $d_{33,f}$ was the ion self bias of the substrate holder, meaning the ion energy and flux of the bombarding species (Ar^+, N^{2+}) [34]. Besides process influence, a distinct influence of the substrate was observed as well. The crystalline order of the latter may influence AlN nucleation in favor of or against (0001) orientation. According to Table 2, AlN and ZnO thin films exhibit quite similar piezoelectric properties. The transverse coefficient is almost equal, while the longitudinal effect is somewhat larger in ZnO. The ZnO thin film properties given in Table 2 are close to single crystal values. In the case of AlN there are no single crystal reference data available.

Table 2. Thin film piezoelectric and dielectric properties.

Coefficients/figures of merit	ZnO [40, 41]	AlN [31, 42]	PZT (1–3 μm) [43]
$e_{31,f}$ (Cm^{-2})	−1.0	−1.05	−8 .. −12
$d_{33,f}$ (pm/V)	5.9	3.9	60 130
ε_{33}	10.9	10.5	300 .. 1300
$e_{31,f}/\varepsilon_0\varepsilon_{33}$ (GV/m)	−10.3	−11.3	−0.7 .. −1.8
$e^2_{31,f}/\varepsilon_0\varepsilon_{33}$ (GPa)	10.3	11.9	6 .. 18
$\tan\delta$ (@1 to 10 kHz, 10^5 V/m)	0.01 .. 0.1	0.003	0.01 .. 0.03
$e_{31,f}/sqrt(\varepsilon_0\varepsilon_{33}\tan\delta)$ (10^5 $Pa^{1/2}$)	3 .. 10	20	4 .. 8
c^E_{33} (GPa) (PZT52/48 ceramic)	208	395	98
$d^2_{33,f}\cdot c^E_{33}/\varepsilon_0\varepsilon_{33}$	7.4 %	6.5%	7% .. 15%

AlN has two major advantages over ZnO. First, it is perfectly compatible with silicon semiconductor technology, whereas Zn, as a fast diffusing ion, is problematic. Secondly, AlN is a large band gap (6 eV) material with a large resistivity, whereas ZnO is really a semiconductor (3.0 eV) with the inherent risks that off-stoichiometry might lead to doping (as e.g. Zn interstitials [35]) and thus to an increased conductivity. It is, in fact, difficult to obtain ZnO with a high resistivity. The dc conductivity translates into a high dielectric loss at low frequencies, which is especially harmful for sensors and actuators working at frequencies below about 10 kHz. The fact that more MEMS studies have been performed with ZnO than with AlN is explained by the better availability of ZnO films, the less demanding vacuum conditions for ZnO, and some early negative experiences with mechanical stresses in AlN thin films. This is, however, not a problem when using modern magnetron sources and careful tuning of ion bombardment impact. The two materials are compared in Table 2 on the basis of measured thin film properties. An accurate method to determine $d_{33,f}$ consists of utilizing a double side laser interferometer, which measures the thickness change unambiguously and avoids errors due to sample deflections [36]. The $e_{31,f}$ coefficient is determined by means of deflecting or deflected structures. The various methods are listed in [37] and [38]. The data on ZnO are based on SAW experiments. MEMS type deflective devices where the ZnO is grown on metal layers typically show smaller $e_{31,f}$ values of typically $-0.6\,C/m^2$ [39]. Table 2 shows that AlN is better suited for deflection devices (especially as sensors), while ZnO should yield larger coupling coefficients for longitudinal bulk acoustic wave generation.

Ferroelectric Thin Films

In other devices, maximizing the piezoelectric coefficient is of considerable importance in reducing the drive voltage or increasing the speed or sensitivity of a MEMS device. For example, in a piezoelectrically-actuated switch for rf signals, the overall speed of the device is limited by the device size, with smaller dimensions yielding higher resonance frequencies. However, since it is imperative that a certain standoff be maintained, in order to maintain a good "on–off" ratio at high frequencies, while the device must be laterally small, it should still be possible for a vertical gap (ideally of several microns) to be maintained [44]. This can

be achieved at modest driving voltages if the actuator piezoelectric coefficient is large.

For applications where large thin film piezoelectric coefficients are required, ferroelectric compositions are extremely attractive. However, this comes at some cost in terms of complexity of the actuator composition (e.g. the necessity for 2–5 cations), need to develop film deposition routes that maintain stoichiometry, phase, and in some cases, orientation, and challenges associated with bringing new materials sets into cleanrooms. Thankfully, the piezoelectric MEMS community can benefit from the tremendous infrastructure development resulting from ferroelectric nonvolatile access memories, which should speed implementation of ferroelectrics-based MEMS devices. This section will detail the available literature on the piezoelectric properties of ferroelectric thin films, with emphasis on the importance of morphotropic phase boundaries and high transition temperatures for MEMS applications.

In ferroelectric materials, there are several contributions to the available piezoelectric response. The intrinsic piezoelectric response is the response that would be made due to application of an electric field to an appropriately averaged ensemble of single crystals. The extrinsic response is typically associated with motion of non-180° domain walls or of phase boundaries. In thin films, the extrinsic contribution to the piezoelectric coefficient is considerably reduced relative to bulk materials [45, 46, 52]. This limits the magnitude of the piezoelectric coefficient that is available in randomly oriented films. However, it has been demonstrated that the intrinsic piezoelectric coefficients are dependent on crystallographic orientation [47]. In particular, many rhombohedrally-distorted perovskites, when poled and driven along the crystallographic [001], have extremely high piezoelectric coefficients [48]. In contrast, in some of the tetragonal perovskites, the piezoelectric response is maximized when measured along the polar axis. As a result, it is extremely interesting to compare the properties of randomly oriented to textured films to see if the same enhancement of the piezoelectric coefficient transfers to thin film samples. Orientation can be controlled by deposition conditions, heating rate, and substrate choice, among other factors.

Morphotropic Phase Boundaries

The most widely utilized ferroelectric thin films for piezoelectric applications are based on lead zirconate

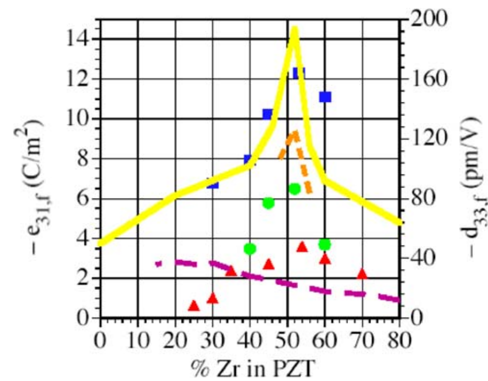

Fig. 3. Composition dependence of the relative piezoelectric response in PZT thin films. Data from [50–54, 56]. Symbols are for $e_{31,f}$ data, lines are for $d_{33,f}$ data.

titanate (PZT). This system illustrates many of the important features of the other ferroelectric compositions, so emphasis will be placed on this family. The lead zirconate titanate phase diagram is dominated by a rhombohdrally distorted ferroelectric region at low Zr contents, a tetragonal region at high Ti concentrations, separated by a morphotropic phase boundary (MPB), with a sliver of monoclinically distorted perovskite at lower temperatures near the MPB [49]. In bulk ceramics, maxima in the piezoelectric d and e coefficients are generally observed at the MPB. The same behavior is often [50–54], but not universally [55, 56] reported in thin films (see Fig. 3). At present there does not appear to be a strong correlation between factors like deposition method (e.g. not all films deposited by chemical solution deposition show comparable composition dependence), film orientation, or film thickness with whether or not strong enhancement of properties is observed at the MPB. Perhaps some of these differences can be ascribed to the effect of grain size, or the relative poling efficiency in films of different compositions.

For good piezoelectric response, it is important not only that a system display a morphotropic phase boundary, but what the transition temperature at the morphotropic phase boundary is. Of course, the magnitude of the piezoelectric coefficient can be enhanced if a system with a low transition temperature is utilized. However, this comes at the expense of heightened temperature dependence in the piezoelectric response, increased tendency towards depoling, and often limitations on the available drive levels due to low coercive fields [57]. Consequently, it is interesting to consider systems that show morphotropic phase

boundaries with high transition temperatures. In the lead-based perovskites, the highest transitions temperatures at known morphotropic phase boundaries occur in the PZT and $PbYb_{1/2}Nb_{1/2}O_3$-$PbTiO_3$ systems. In both cases, the transition temperatures are near 360°C at the MPB. Even higher transition temperature MPB compositions have been reported recently in $BiMeO_3$-$PbTiO_3$ solid solutions. High piezoelectric coefficients ($d_{33} = 465$ pC/N) have been measured in bulk ceramic $BiScO_3$-$PbTiO_3$ 36/64 with transition temperatures of 450°C [57, 58]. While the transition temperatures of thin films can differ from those of bulk ceramic materials, as a rule of thumb, for the large film thicknesses required in many MEMS devices, the transition temperatures are often reasonably close (often within ∼50°C) to those observed in bulk ceramics and single crystals. Consequently, the high T_c MPB ceramics offer a good guide as to the materials that will be interesting for high T_c, high piezoelectric activity piezoelectric thin films.

Effect of Film Orientation

There are discrepancies in the literature concerning whether or not there is a strong orientation dependence of the piezoelectric properties in ferroelectric thin films. For example, various authors have reported maxima for {111}, {100}, or randomly oriented PZT films near the morphotropic phase boundary [51, 52, 59]. It is possible that the differences are related to changes in the film domain state, perhaps due to residual stresses. Certainly, the piezoelectric response does appear to correlate with the magnitude of the remanent polarization; films with low remanent polarizations have low piezoelectric coefficients. This may also indicate the importance of grain size in ferroelectric thin films, especially for films under tensile stress. As has been shown by Tuttle and co-workers [60], in many thin films, the domain state is governed substantially by the stress experienced by the film during cooling through the phase transformation temperature. Consequently, perovskite structured thin films, when exposed to tensile stresses during the cooling process, tend to have their polar vectors in orientations approximately parallel to the substrate (of course constrained by the crystallography of the system); films under compressive stresses tend to have the polarization oriented more nearly perpendicular to the substrate. Because the mobility of non-180° domain walls in ferroelectric thin films tends to be limited compared to bulk materials, once the ferroelastic domain orientation is established, it is difficult to change at room temperature [45, 61]. Larger grained films tend to show more complicated domain structures within a single grain [60], and so may be less susceptible to reduction in the remanent polarization and piezoelectric response.

PZT film processing offers the possibility to achieve textured films. Growth of PZT is strongly nucleation controlled, meaning that the nucleation can be manipulated to achieve a desired orientation. On a perovskite single crystal substrate or electrode, PZT grows almost inevitably in the same orientation as the template. On platinum this is less evident. Platinum films are most often deposited with a (111) texture. As the lattice constant of Pt is rather close to that of PZT (2–3% mismatch), one could expect that PZT tends to grow with a (111) orientation on Pt. This is, however, not necessarily so. A mixture of all major orientations is obtained in the general case. Control of the orientation by using thin buffer layers has been reported to be successful in sputtered films on Pt-coated substrates. For example, $PbTiO_3$ will often adopt a (100) orientation on Pt, and serve as a template for well-oriented PZT films, while a thin TiO_2 buffer layer can yield (111) oriented perovskites [62]. During sol-gel film processing, the concentration of excess lead, the pyrolysis temperature, as well as the ramp speed used in the rapid thermal annealing all play a substantial role for orientation control [63]. The temporary formation of a Pt_3Pb interface layer has been identified as a mechanism promoting (111) orientation [64, 65]. Texture control is important for obtaining optimal properties. PZT {100} films show substantially larger piezoelectric responses than those of {111} films, as shown in Fig. 4.

Similar orientation-induced enhancements in the piezoelectric response have been reported in a number of perovskite solid solutions. In particular, high piezoelectric coefficients have been reported in {001} films (on the rhombohedral side of the morphotropic phase boundary) in $PbMg_{1/3}Nb_{2/3}O_3$-$PbTiO_3$ (PMN-PT) [66, 67] $PbYb_{1/2}Nb_{1/2}O_3$-$PbTiO_3$ [78] and $BiScO_3$-$PbTiO_3$ [78, 79]. For example, in PMN-PT 70/30 films on Si, the ratio of the piezoelectric response for {100} oriented films, relative to {111} ranged from 1.6–1.9 [66], with a maximum $e_{31,f}$ coefficient of -5.5 C/m^2. In both PYbN-PT 50/50 and 60/40 epitaxial films on $SrRuO_3$/$SrTiO_3$, $e_{31,f}\{100\}/e_{31,f}\{111\}$ was ∼3.6 (see Fig. 5). For the {100} films, $e_{31,f}$ values of -14 C/m^2 to -19 C/m^2 were obtained in films of 1 and 3 microns thickness, respectively [68, 78]. For the

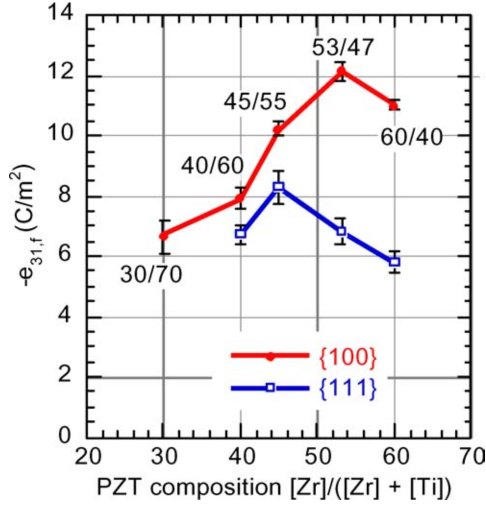

Fig. 4. Transverse piezoelectric response in {111} and {100} textured PZT films as a function of composition. All of the films were deposited on Pt-coated Si substrates. Data from [43].

$BiScO_3$-$PbTiO_3$ films, $e_{31,f}$ of -9 to -12 C/m^2 have been achieved in {100} epitaxial films [78, 79]. This is especially encouraging, because the high piezoelectric response is coupled with a high transition temperature of ~460°C (~100°C higher than at the PZT morphotropic phase boundary). In general, for films that show enhanced piezoelectric response with orientation (of the type predicted based on phenomenology [47, 69]), the achieved anisotropy in directly related to the quality of the orientation. Thus, many of the epitaxial films show stronger anisotropy than fiber textured films (where the percentage of oriented material may be substantially reduced—see for comparison [70, 71, 78]. This type of orientation-enhanced piezoelectric response is especially useful in thin films, as ferroelastic domain wall motion is so heavily clamped.

It is critical to note, however, that orientation itself, does not guarantee large piezoelectric response. This is clear in a comparison of lead magnesium niobate—lead titanate films grown on Si with those grown on most single crystal oxide substrates. Films grown on Si generally have low remanent polarization values (~10 μC/cm^2), and consequently, low $e_{31,f}$ values when poled through the film thickness. This is largely because the tensile stress in the films resulting from the mismatch in thermal expansion coefficients rotates the hysteresis loop clockwise [72]. The result is low remanent piezoelectric response. In contrast, films grown on single crystal oxide substrates such as $SrTiO_3$ or $LaAlO_3$, show much squarer hysteresis loops, and larger piezoelectric coefficients [67, 73]. It is important to note that this is not just a consequence of crystal quality or epitaxy. Thus, when the elastic constraints imposed by the substrate are removed, the remanent polarization and $e_{31,f}$ coefficients of epitaxial PMN-PT films on Si increase substantially [67]. While some of the relaxor-based materials such as PMN-PT appear to be especially sensitive to imposed stresses, similar stress-induced rotations of the hysteresis loops have

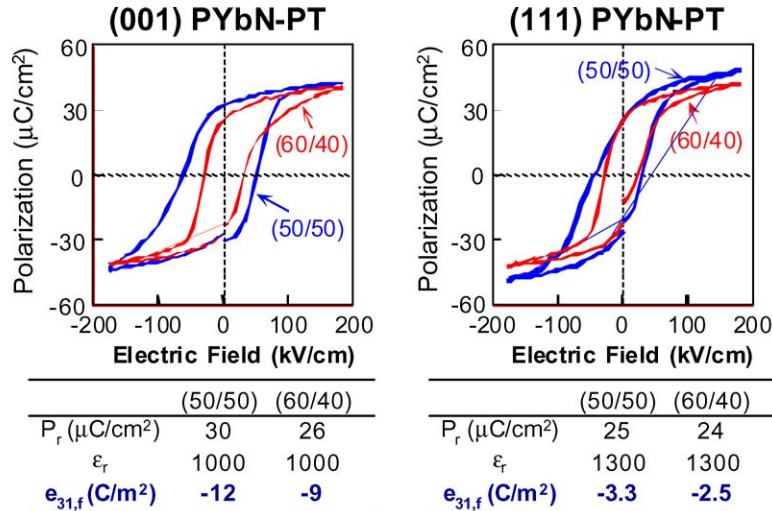

(001) PYbN-PT

	(50/50)	(60/40)
P_r (µC/cm²)	30	26
ε_r	1000	1000
$e_{31,f}$ (C/m²)	**-12**	**-9**

(111) PYbN-PT

	(50/50)	(60/40)
P_r (µC/cm²)	25	24
ε_r	1300	1300
$e_{31,f}$ (C/m²)	**-3.3**	**-2.5**

Fig. 5. Piezoelectric anisotropy in PYbN-PT epitaxial films. Data from [78].

been observed in PZT [74]. Thus, it is likely that the behavior is rather general.

In addition to orientation, the piezoelectric properties of ferroelectric materials including PZT are strongly influenced by composition, grain size, defect chemistry, and mechanical boundary conditions [75–77]. This is one area where film deposition conditions and substrate choice can strongly impact the quality of the resulting materials. For example, it has been suggested that small grain size can lead to grains where a limited number of domain variants are observed [60]. The result for films on Si can be lower remanent polarizations, and suppressed extrinsic contributions to the available piezoelectric response [45, 60]. In many polycrystalline films, the lateral grain size is controlled by the grain size of the underlying Pt electrode. Since the latter is often quite fine, it is not uncommon for film grain sizes to be in the range of 50–200 nm. If, however, the deposition conditions have been optimized so that nucleation is not dominated by the electrode crystallites, then larger grain sizes can result.

A second important factor is substrate-dominated changes in the observed piezoelectric response. As explained in the section on piezoelectric coefficients, thin films are mechanically clamped by a massive substrate. The composition of the substrate would be expected to be important both due to differences in the thermal expansion coefficient (and hence the resulting film stress) and due to the importance of the substrate elastic moduli in controlling the mechanical boundary conditions of the film. There has been relatively little literature on the importance of the substrate in controlling the magnitude of the piezoelectric response. This may be in part because it is so difficult to control the microstructure of the ferroelectric film independent of the substrate. Work by Dubois suggests that for a given film microstructure and poling state, the magnitude of the $e_{31,f}$ coefficient increases with applied static tensile strains, and decreases for applied compressive strains [38]. Figure 6 shows a comparison of the piezoelectric responses of thin film and bulk PZT ceramics, highlighting the importance of elastic boundary conditions. 3 to 4 μm thick PZT films are close to the performance calculated for a standard hard ceramics, the PZT 4D. However, their response falls below the $e_{31,f}$ of the optimized, rather soft ceramics (Motorola 3203D) by a factor of two. It is noteworthy that an increase in film thickness increases $d_{33,f}$ significantly, but does not improve $e_{31,f}$. Such behavior could be explained if porosity increases with thickness: substrate effects

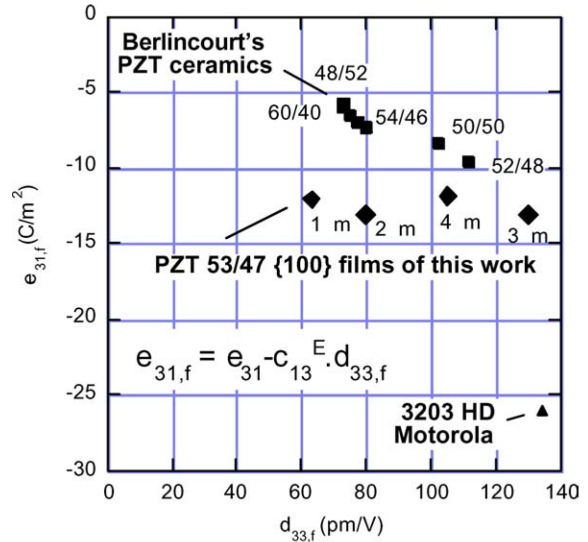

Fig. 6. PZT thin films compared to bulk ceramics values: $e_{31,f}$ vs. $d_{33,f}$. Data from [43].

are reduced—increasing $d_{33,f}$—and in-plane stiffness is reduced as well—decreasing $e_{31,f}$. However, TEM and SEM inspections do not support the idea of increased porosity. This effect is thus very likely related to a mechanism of elastic domains that can move more easily in thicker films, and that give rise to out-of-plane strain, but not to in-plane strain (rhombohedral symmetry).

Figure 7 shows a comparison of the available data in the literature on morphotropic phase boundary ferroelectrics. The low transition temperature compounds ($<200°$C) are PMN-PT materials, the films near 350–420°C are either PZT or PYbN-PT, while the highest transition temperature data are for $BiScO_3$-$PbTiO_3$ films. The substrates range from single crystal oxides (e.g. $LaAlO_3$ or $SrTiO_3$) to Si. In all cases where data were reported, the measured transition temperatures (rather than the bulk numbers) were used in the plot. This was done since the transition temperatures in films depend on the levels of stress the film is under and the composition (including A:B site ratio). It is clear that the highest piezoelectric coefficients are shown in oriented thin films on the rhombohedral side of the morphotropic phase boundary, suggesting that the domain rotation argument proposed for bulk single crystals applies to thin films as well. In addition, it is clear that the magnitude of the piezoelectric coefficient depends somewhat on film thickness, with the highest

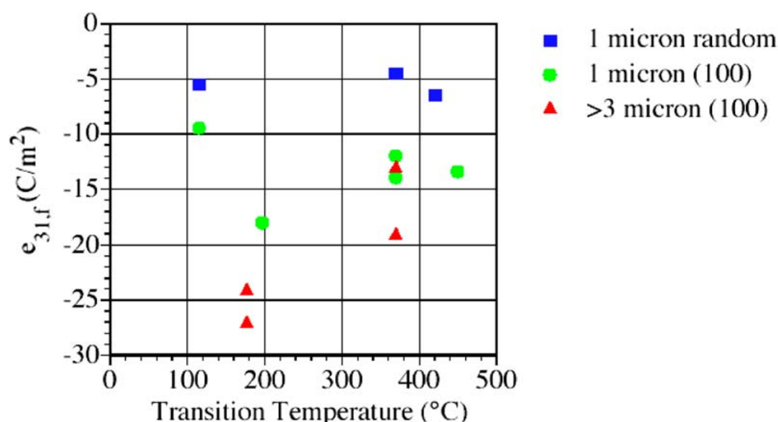

Fig. 7. Piezoelectric coefficients of a number of morphotropic phase boundary ferroelectric thin films plotted as a function of the measured transition temperature. Data from [15, 52, 67, 73, 78, 79].

piezoelectric constants being reported for thicker films.

Conclusions

This paper reviews the current state of piezoelectric thin films for microelectromechanical systems. Over the last 15 years, considerable progress has been made in optimizing the deposition conditions for thin films to improve the available piezoelectric activity. Control of the growth process is essential in the wurtzite-structured materials, since the polarization direction cannot be switched following deposition. The resulting materials show good temperature stability and the response, coupled with smaller piezoelectric coefficients. Much larger $e_{31,f}$ values can be achieved in many of the ferroelectric compositions. The resulting properties are dependent on film grain size, thickness, and orientation, with the best responses reported to date in $\{001\}$ oriented films near the morphotropic phase boundary.

References

1. F.D. Bannon, J.R. Clark, and C.T.C. Nguyen, *IEEE J. Sol. State Circuits*, **35**(4), 512 (2000).
2. L.W. Lin, R.T. Howe, and A.P. Pisano, *J. MEMS*, **7**(3), 286 (1998).
3. L. Pescini, H. Lorenz, and R.H. Blick, *Appl. Phys. Lett.* **82**(3), 352 (2003).
4. M.A. Abdelmoneum, M.U. Demirci, and C.T.-C. Nguyen, *The Sixteenth Annual International Conference on Micro Electro Mechanical Systems, 2003*. MEMS-03 Kyoto. IEEE, 698 (2003).
5. Y. Ito, K. Kushida, K. Sugawara, and H. Takeuchi, *IEEE TUFFC*, **42**, 316 (1995).
6. M.A. Dubois and P. Muralt, *Appl. Phys. Lett.*, **74**, 3032 (1999).
7. S.H. Kim, J.H. Kim, H.D. Park, and G.W. Yoon, *J. Vac. Sci. Tech.* B, **19**, 1164 (2001).
8. M. Umeda, K. Nakamura, and S. Ueha, *Jpn. J. Appl. Phys. Part 1*, **36**(5B), 3146 (1997).
9. G.W. Taylor, J.R. Burns, S.M. Kammann, W.B. Powers, and T.R. Welsh, *IEEE J. Ocean. Eng.*, **26**(2), 539 (2001).
10. G.K. Ottman, H.F. Hofmann, and G.A. Lesieutre, *IEEE Trans. Power Electron.*, **18**(2), 696 (2003).
11. P. Glynne-Jones, S.P. Beeby, and N.M. White, *IEE Proc. Sci. Meas. Tech.,* **148**(2) 68 (2001).
12. J.J. Bernstein, S.L. Finberg, K. Houston, L.C. Niles, H.D. Chen, L.E. Cross, K.K. Li, and K. Udayakumar, *IEEE Trans. UFFC*, **44**, 960 (1997).
13. Y. Nemirovsky, A. Nemirovsky, P. Muralt, and N. Setter, *Sen. and Act.*, **A56**, 239 (1996).
14. P. Muralt, M. Kohli, T. Maeder, A. Kolkin, K. Brooks, N. Setter, and R. Luthier, *Sen. and Act.*, **A48**, 157 (1995).
15. P. Muralt, *IEEE Trans. UFFC*, **47**(4), 903 (2000).
16. D.L. Polla and L.F. Francis, *MRS Bulletin*, **21**(7), 59 (1996).
17. L.-P. Wang, K. Deng, L. Zou, R. Wolf, R.J. Davis, and S. Trolier-McKinstry, *IEEE Electron Device Lett.*, **23**, 182 (2002).
18. J.F. Nye, *Physical Properties of Crystals: Their Representation by Tensors and Matrices* (Clarendon Press, Oxford, 1979).
19. T. Ikeda, *Fundamentals of Piezoelectricity* (Oxford University Press, New York, 1996).
20. R.M. White and V.W. Voltmer, *Appl. Phys. Lett.*, **17**, 314 (1965).
21. K. Tsubouchi and N. Mikoshiba, *IEEE Trans. Son. Ultrasonics*, **32**, 634 (1985).
22. H. Nakahata, H. Kitabayashi, T. Uemura, A. Hachigo, K. Higaki, S. Fujii, Y. Seki, K. Yoshida, and S. Shikata, *Jpn. J. Appl. Phys. Pt 1*, **37** 2918 Sp. Iss. SI (1998).
23. G.F. Iriarte, *J. Appl. Phys.*, **93**, 9604 (2003).

24. I. Cerven, T. Lacko, I. Novotny, V. Tvarozek, and M. Harvanka, *J. Cryst. Growth*, **131**(3/4), 546 (1993).
25. J.G. Smits and W.S. Choi, *IEEE TUFFC*, **38**(3), 256 (1991).
26. Q. Meng, M. Mehregany, and K. Deng, *J. Micromech. Microeng.*, **3**, 18 (1993).
27. Ph. Luginbuhl, G.-A. Racine, Ph. Lerch, B. Romanowicz, K.G. Brooks, N.F. de Rooij, Ph. Renaud, and N. Setter, *Int. Conf. Solid-State Sens. Act., Proc.*, **1**, 413 (1995).
28. T. Fabula, H. Wagner, B. Schmidt, and S. Buttgenbach, *Sens. Act. A*, **42**(1–3), 375 (1994).
29. F.S. Hickernell, *Proc. IEEE*, **64**, 631 (1976).
30. A. Rodriguez-Navarro, W. Otano-Rivera, J.M. Garcia–Ruiz, and R. Messier, *J. Mater. Res.*, **12**, 1850 (1997).
31. M.A. Dubois and P. Muralt, *Appl. Phys. Lett.*, **74**(20), 3032 (1999).
32. F.J. Hickernell, R.X. Yue, and F.S. Hickernell, *IEEE Trans. UFFC*, **44**, 615 (1997).
33. H.P. Loebl, C. Metzmacher, R.F. Milsom, P. Lok, F. van Straten, and A. Tuinhout, *J. Electroceramics*, forthcoming issue.
34. M.-A. Dubois and P. Muralt, *J. Appl. Phys.*, **89**, 6389 (2001).
35. A. Barker, S. Crowther, and D. Rees, *Sensors & Actuators*, **58**, 229 (1997).
36. A.L. Kholkin, C. Wutchrich, D.V. Taylor, and N. Setter, *Rev. Sci. Instrum.*, **67**(5), 1935 (1996).
37. J.F. Shepard, Jr., P.J. Moses, and S. Trolier-McKinstry, *Sens. Actuators A*, **71**, 133 (1998).
38. M.A. Dubois and P. Muralt, *Sens. Act. A*, **77**(20), 106 (1999).
39. F.J. von Preissig, H. Zeng, and E.S. Kim, *Smart Mater. Struct.*, **7**, 396 (1998).
40. J.G. Gualtieri, J.A. Kosinski, and A. Ballato, *Trans. UFFC*, **41**, 53 (1994).
41. G. Carlotti, G. Socino, A. Petri, and E. Verona, *Proc. 1987 IEEE Ultrason. Symp.* (Oct. 1987), p. 295.
42. K. Tsubouchi, K. Sugai, and N. Mikoshiba, *IEEE Ultrason. Symp.*, Oct. 1981, p. 375.
43. N. Ledermann, P. Muralt, J. Baborowski, S. Gentil, K. Mukati, M. Cantoni, A. Seifert, and N. Setter, *Sens. Act. A*, **105**, 162 (2003).
44. D. Peroulis, S.P. Pacheco, K. Sarabandi, and L.P.B. Katehi, *IEEE Trans. Microwav. Theory Tech.*, **51**(10), 259 (2003).
45. F. Xu, S. Trolier-McKinstry, W. Ren, and B. Xu, *J. Appl. Phys.*, **89**(2), 1336 (2001).
46. K. Saito, T. Kurosawa, T. Akai, T. Oikawa, and H. Funakubo, *J. Appl. Phys.*, **93**(1), 545 (2003).
47. X.H. Du, J.H. Zheng, U. Belegundu, and K. Uchino, *Appl. Phys. Lett.*, **72**(19), 2421 (1998).
48. S.-E. Park and T.R. Shrout, *IEEE Trans. UFFC*, **44**, 1140 (1997).
49. B. Noheda, D.E. Cox, G. Shirane, R. Guo, B. Jones, and L.E. Cross, *Phys. Rev. B*, **63**(1), 014103 (2001).
50. H.D. Chen, K.R. Udayakumar, C.J. Gaskey, and L.E. Cross, *Appl. Phys. Lett.*, **67**(23), 3411 (1995).
51. A. Seifert, N. Ledermann, S. Hiboux, J. Baborowski, P. Muralt, and N. Setter, *Integr. Ferro.*, **35**(1–4), 1889 (2001).
52. F. Xu, R.A. Wolf, T. Yoshimura, and S. Trolier-McKinstry, *Proc. 11th Int. Symp. Electrets*, 386 (2002).
53. R.A. Wolf and S. Trolier McKinstry, *J. Appl. Phys.*, **95**(3), 1397 (2004).
54. T. Haccart, C. Soyer, E. Cattan, and D. Remiens, *Ferroelectrics*, **254**(1–4), 185 (2001).
55. I. Kanno, H. Kotera, K. Wasa, T. Matsunaga, T. Kamada, and R. Takayama, *J. Appl. Phys.*, **93**(7), 4091 (2003).
56. D.-J. Kim, J.-P. Maria, A.I. Kingon, and S.K. Streiffer, *J. Appl. Phys.*, **93**, 5568 (2003).
57. R.E. Eitel, C.A. Randall, T.R. Shrout, P.W. Rehrig, W. Hackenberger, and S.E. Park, *Jpn. J. Appl. Phys. Part 1*, **40**(10), 5999 (2001).
58. T.R. Shrout, Private Communication (2002).
59. K. Kakimoto, H. Kakemoto, S. Fujita, and Y. Masuda, *J. Am. Ceram. Soc.*, **85**(4), 1019 (2002).
60. B.A. Tuttle, T.J. Garino, J.A. Voight, T.J. Headley, D. Dimos, and M.O. Eatough, *Science and Technology of Electroceramic Thin Films*, edited by O. Auciello and R. Waser, Kluwer Academic Publishers, The Netherlands, 117 (1995).
61. A.L. Kholkin, M.L. Calzada, P. Ramos, J. Mendiola, and N. Setter, *Appl. Phys. Lett.*, **69**, 3602 (1996).
62. P. Muralt, *J. Micromech. Microeng.*, **10**, 136 (2000).
63. K.G. Brooks, I.A. Reaney, R. Klissurska, Y. Huang, L. Bursill, and N. Setter, *J. Mater. Res.*, **9**, 2540 (1994).
64. S.-Y. Chen and I.-W. Chen, *J. Amer. Cer. Soc.*, **77**, 2337 (1994).
65. R.W. Whatmore, Q. Zhang, Z. Huang, and R.A. Dorey, *Materials Science in Semiconductor Processing*, **5**, 65 (2003).
66. J.H. Park, F. Xu, and S. Trolier-McKinstry, *J. Appl. Phys.*, **89**(1), 568 (2001).
67. D.M. Kim, S.D. Bu, C.B. Eom, S. K. Streiffer, W. Tian, X.Q. Pan, T. Yoshimura, S. Trolier-McKinstry, D.G. Schlom, V. Nagurajan, A. Stanishev-Sky, J. Ouyang, R. Ramash, W. Tian, and X.Q. Pan, *unpublished*.
68. T. Yoshimura and S. Trolier-McKinstry, *Integr. Ferroelectr.*, **50**, 33 (2002).
69. A.J. Bell, *J. Appl. Phys.*, **89**(7), 3907 (2001).
70. Q.Q. Zhang, Q.F. Zhou, and S. Trolier-McKinstry, *Appl. Phys. Lett.*, **80**(18), 3370 (2002).
71. Q.F. Zhou, Q.Q. Zhang, and S. Trolier-McKinstry, *J. Appl. Phys.*, **94**(5) 3397 (2003).
72. Z. Zhang, J.-H. Park, and S. Trolier-McKinstry, *MRS. Proc. 596 Ferroelectric Thin Films VIII*, edited by R.W. Schwartz, P.C. McIntyre, Y. Miyasaka, S.R. Summerfelt, and D. Wouters, Materials Research Society, Warrendale, PA, 73, (2000).
73. J.P. Maria, *Ph.D. Thesis*, The Pennsylvania State University (1998).
74. J.F. Shepard Jr., S. Trolier-McKinstry, M. Hendrickson, and R. Zeto, *MRS Proc. 459: Materials for Smart Systems II*, 47 (1997).
75. N. Kim, Ph. D. Thesis, The Pennsylvania State University (1994).
76. F. Jona and G. Shirane, *Ferroelectric Crystals* (Pergamon Press, New York, 1962).
77. T.M. Shaw, S. Trolier-McKinstry, and P.C. McIntyre, *Ann. Rev. Mater. Sci.*, **30**, 263 (2000).
78. T. Yoshimura and S. Trolier-McKinstry, *J. Appl. Phys.*, **92**(7), 3979 (2002).
79. J. Nino, T. Yoshimura, and S. Trolier-McKinstry, *J. Mat. Res.* (2003), submitted.